

Article

Pore Types and Characteristics of Ultra-Deep Shale of the Lower Paleozoic Wufeng-Longmaxi Formations in the Eastern Sichuan Basin

Ruolong Chi ¹, Ping Gao ^{1,*} , Yidong Cai ¹, Ruobing Liu ², Jinghan Du ¹ and Qin Zhou ³

¹ School of Energy Resources, China University of Geosciences, Beijing 100083, China; rlong0131@163.com (R.C.); yidong.cai@cugb.edu.cn (Y.C.); 1006192317@cugb.edu.cn (J.D.)

² Sinopec Exploration Branch Company, Chengdu 610041, China; liurb.ktnf@sinopec.com

³ State Key Laboratory of Organic Geochemistry, Guangzhou Institute of Geochemistry, Chinese Academy of Sciences, Guangzhou 510640, China; qzhou@gig.ac.cn

* Correspondence: gaoping1212@cugb.edu.cn

Abstract: Recently, shale gas exploration of the Wufeng-Longmaxi formations (WF-LMX) in the Sichuan Basin has gradually stepped into deep to ultra-deep layers, but the pore types and characteristics of ultra-deep shale still remain unclear. In this study, the WF-LMX ultra-deep organic-rich shale samples in the Eastern Sichuan Basin were collected, and the types and development characteristics of shale pores were investigated by using high-resolution scanning electron microscopy (SEM). Our results showed that the pores of the WF-LMX ultra-deep shale reservoirs mainly included organic pores, mineral matrix pores (interparticle pores and intraparticle pores), and micro-fractures, which were dominated by organic pores, displaying oval, slit, and irregular shapes and a diameter of mainly 5–45 nm. Organic pores were poorly developed in primary organic matter (e.g., graptolite and radiolarian), while they were well developed in solid bitumen, being the most important nanopore type in shale. The pore development of ultra-deep shale was mainly controlled by the contents of organic matter and brittle minerals. Higher contents of organic matter and quartz are conducive to the development and preservation of organic pores, which are also favorable for ultra-deep shale gas exploration.

Keywords: nanopore; organic pore; quartz; shale gas



Citation: Chi, R.; Gao, P.; Cai, Y.; Liu, R.; Du, J.; Zhou, Q. Pore Types and Characteristics of Ultra-Deep Shale of the Lower Paleozoic Wufeng-Longmaxi Formations in the Eastern Sichuan Basin. *Energies* **2023**, *16*, 6102. <https://doi.org/10.3390/en16176102>

Academic Editor: Pål Østebø Andersen

Received: 18 July 2023

Revised: 13 August 2023

Accepted: 19 August 2023

Published: 22 August 2023



Copyright: © 2023 by the authors. Licensee MDPI, Basel, Switzerland. This article is an open access article distributed under the terms and conditions of the Creative Commons Attribution (CC BY) license (<https://creativecommons.org/licenses/by/4.0/>).

1. Introduction

In the past few decades, shale gas has been commercially produced in many countries and regions, such as North America and China, due to the application of horizontal drilling and hydraulic fracturing technologies [1,2]. Shale gas, which has been proven to be abundant in China, is widely distributed in marine, transitional, and lacustrine shale successions from the Precambrian to the Neogene. Among them, marine shales account for the largest proportion of total shale gas yields, i.e., $13 \times 10^{12} \text{ m}^3$ [3,4]. Shale gas mainly exists in micro- and nano-scale pores of organic matter via adsorbed and free phases, which is a kind of self-generated, self-stored, and continuously distributed unconventional gas [5–7]. The pores of gas shale reservoirs are mainly micro- to nano-scaled [8]. The porosity and permeability of gas shale reservoirs are low, and shale pore structure exhibits high degrees of complexity and strong heterogeneity [9–11]. The characteristics and types of micro- and nano-scaled pore structure in shale reservoirs exert an important effect on the adsorption capacity and migration of methane gas and play an important role in the prediction of shale gas reserves as well as the exploration and development of shale gas. Using argon-ion polished shale samples and high-resolution field emission scanning electron microscopy (FE-SEM), various authors have found a variety of pore types and proposed pore classification schemes [12–14]. For example, Slatt and O'Brien characterized

the pore types of the Barnett and Woodford shale reservoirs and divided the shale pores into six types [12]. Loucks et al. proposed a ternary classification scheme of shale pores, mainly including mineral matrix pores (interparticle pores, intraparticle pores), organic matter (OM) pores, and fracture pores [13]. Numerous studies on the pore characterization of gas shale reservoirs have suggested that the OM-hosted pores have significant contributions to the shale pore system [14–16].

According to the current technical level of shale gas exploration, gas shale with a burial depth greater than 3500 m can be divided into deep shale (3500–4500 m) and ultra-deep shale (4500–6000 m) [17,18]. The “United States shale revolution” has greatly promoted the exploration and development of shale gas in China, and a major breakthrough in the Lower Paleozoic Wufeng-Longmaxi formations (WF-LMX) of the Sichuan Basin and its surrounding areas has been made. [2,19]. At present, the WF-LMX mid-shallow shale deposits with burial depths less than 3500 m have been commercially exploited, and three large shale gas fields, including Jiaoshiba, Weiyuan, and Changning-Zhaotong shale gas fields, have been established [20,21]. In recent years, the exploration and development of the WF-LMX shale gas have gradually stepped into deep and ultra-deep layers [22], and several deep shale gas fields, including the Weirong and Yongchuan shale gas fields, have been discovered. The WF-LMX deep shale in the Sichuan Basin is widely distributed, and the distribution area and geological reserves of deep shale are about twice those of mid-shallow shale [23]. A number of deep shale gas wells in the southern Sichuan Basin have achieved high production, showing that deep shale gas resources are abundant and have broad prospects. The WF-LMX deep shale is becoming an important alternative target for shale gas exploration and development in South China. Moreover, the increase in shale gas production in the future is mainly dependent on the deep marine shale in the Sichuan Basin [24,25]. Recently, an exploration well (PS1 well) in the Eastern Sichuan Basin had been conducted, and the high-quality WF-LMX ultra-deep shale gas reservoirs, with burial depths of 5917.66–5971.00 m average total gas content of 7.74 m³/t, had been found, revealing significant potential for ultra-deep shale gas exploration [26].

The pore types and characteristics of mid-shallow WF-LMX shale reservoirs in the Sichuan Basin have been widely investigated, and numerous studies have found that organic pores are the main pore types in gas-bearing shale, and pore structures of mid-shallow shale are controlled by various geological and geochemical factors, such as total organic carbon (TOC), mineral compositions, kerogen type, maturity, and fluid pressure [27,28]. Since ultra-deep shale has the characteristics of greater burial depth, higher formation temperature and pressure, and high costs of coring, studies on the evaluation of ultra-deep shale reservoirs are relatively weak [29]. In addition, there is little known about the formation mechanism of organic pores in ultra-deep shale reservoirs, confronting a series of theoretical and technical difficulties [30].

Therefore, taking the WF-LMX ultra-deep shale in Eastern Sichuan as the research object, this paper uses high-resolution scanning electron microscopy observation combined with image processing software to systematically study the pore types and morphological characteristics of shale reservoirs, analyze the micro- to nano-scaled pore structure characteristics of shale reservoirs, and explore the main factors controlling the micro-pore structure of shale reservoirs. The evaluation of the micropore structure of ultra-deep shale reservoirs can shed light on the enrichment mechanism of ultra-deep shale gas and play a guiding role in the future exploration and development of marine shale gas in South China.

2. Geological Setting and Studied Well

The Sichuan Basin is a tectonically superimposed basin that is developed on the Upper Yangtze Platform in South China. During the Late Ordovician, a restricted shelf basin surrounded by several uplifts, including the Qianzhong uplift in the south, the Chuanzhong uplift in the west, and the Xuefeng paleo uplift in the east, was formed in the Upper Yangtze Platform due to extensive compression (Figure 1), which was characterized by low-energy, under-compensated, and anoxic sedimentary environments. Moreover,

two successions of anoxic shale deposits (i.e., Wufeng and Longmaxi Formations) were widely formed in this restricted basin due to two global transgressions during the Late Ordovician–Early Silurian.

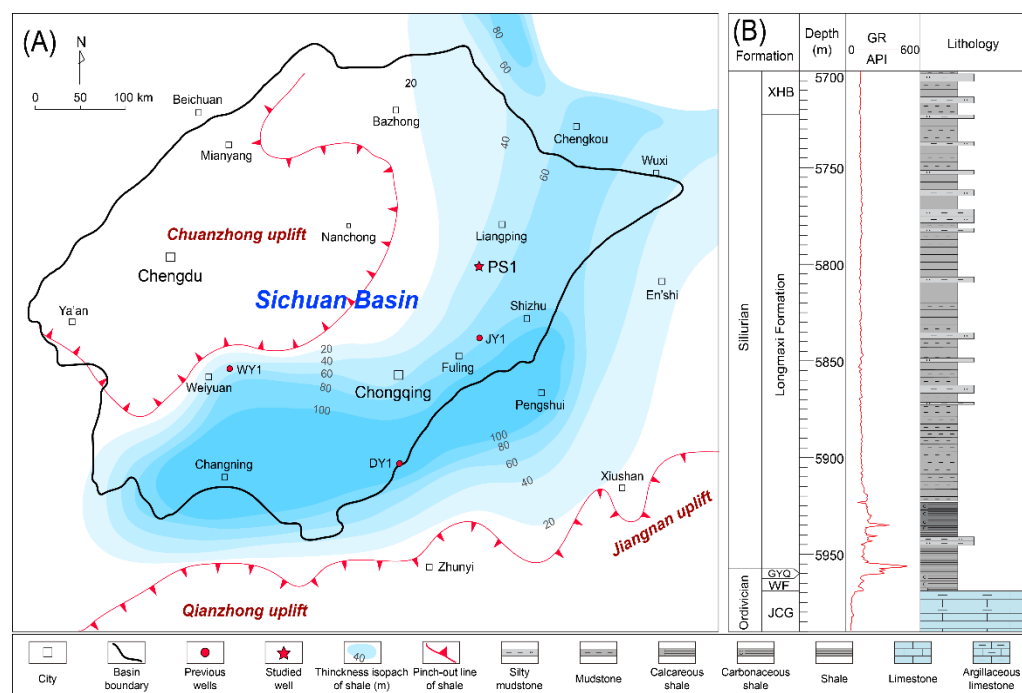


Figure 1. (A) Contour map of the thickness of the Wufeng-Longmaxi formations of organic-rich shales in the Sichuan Basin; (B) Stratigraphic column of the Wufeng-Longmaxi formations for the studied Well PS1 (modified from [25]). JCG = Jiancaogou Formation; WF = Wufeng Formation; GYQ = Guanyinqiao Member; XHB = Xiaoheba Formation.

The studied PS1 well is located in the Eastern Sichuan Basin, and the WF-LMX shale is deposited in semi-deep shelf facies (Figure 1). The Upper Ordovician Wufeng Formation (WF) of Well PS1 is about 15 m thick and is mainly composed of gray-black carbonaceous mudstone with a small amount of gray mudstone. The top of the WF is Guanyinqiao Member (GYQ), with a thickness of only 25 cm, which consists of black-gray argillaceous dolomite containing shell fossils. The Lower Silurian Longmaxi Formation (LMX) is mainly composed of dark gray/black gray mudstone, gray to dark gray silty mudstone intercalated with gray black silty mudstone, and dolomitic mudstone (Figure 1).

3. Materials and Methods

3.1. Materials

A total of 7 shale samples, including 2 WF samples and 5 LMX samples, were collected from the WF-LMX of the Well PS1, Eastern Sichuan Basin, with a burial depth of 5918.36–5964.9 m (Figure 1), and the details of the studied shale samples are shown in Table 1. Total organic carbon (TOC) and mineral compositions of the studied shale samples were compiled from Gao et al. [25].

3.2. Analytical Methods

3.2.1. SEM Observation

Firstly, the shale samples were cut into 1.5 cm × 1 cm × 0.5 cm plugs, and the selected observation section was mechanically polished. Secondly, the observation section was further polished using a Hitachi IM4000 argon ion milling system in order to obtain a highly smooth surface. Finally, the surfaces were observed by a Hitachi S-8000 high resolution cold field emission scanning electron microscope, and secondary electron mode was used to obtain high resolution scanning electron microscope images. During the observation,

the unknown minerals were distinguished by the energy dispersive spectrometer (EDS). Imaging was performed at 1.5 kV and a working distance of 3–4 mm under vacuum. The EDS measurement of candidate minerals was conducted in SE mode with a working distance of 15 mm and a voltage of 15 kV. This work was conducted at the State Key Laboratory of Organic Geochemistry, Guangzhou Institute of Geochemistry, Chinese Academy of Sciences.

Table 1. Basic information on the studied Wufeng-Longmaxi formation shale samples from Well PS1.

| Sample | Depth (m) | Strata | TOC (%) ^a | Mineralogical Composition (%) ^a | | | | | | | Surface Porosity (%) | |
|--------|-----------|--------|----------------------|--|--------------|---------------|-----------|------------|----------|--------|------------------------|--------------------------|
| | | | | Quartz % | K-Feldspar % | Plagioclase % | Calcite % | Dolomite % | Pyrite % | Clay % | Total Surface Porosity | Organic Surface Porosity |
| PS1-02 | 5964.5 | WF | 4.58 | 55.3 | / | 6 | / | 6.6 | / | 32.1 | 0.87 | 0.82 |
| PS1-04 | 5961.1 | WF | 4.66 | 66 | / | 4.7 | / | / | 3 | 26.3 | 0.89 | 0.83 |
| PS1-05 | 5959.2 | LMX | 5.43 | 68.4 | / | 1.9 | 1.6 | 7 | 3 | 18.1 | 1.07 | 0.98 |
| PS1-08 | 5953.5 | LMX | 5.97 | 42.4 | / | 11 | 4.3 | 17.9 | 8 | 16.4 | / | / |
| PS1-13 | 5947.84 | LMX | 2.36 | 41.2 | 2.6 | 9.6 | 2.4 | 8.4 | 2.9 | 32.9 | 0.77 | 0.62 |
| PS1-14 | 5947.06 | LMX | 2.71 | 39.3 | / | 9.5 | 4.2 | 9.1 | 1.6 | 36.3 | 0.82 | 0.69 |
| PS1-22 | 5933.36 | LMX | 3.61 | 32.4 | / | 8.1 | / | 6.6 | 2.5 | 50.4 | / | / |

^a, TOC and mineral compositions were cited from Gao et al. [25].

3.2.2. Surface Porosity Measurement

A threshold segmentation method was adopted in the SEM photographs based on gray-level information of minerals, organic matter, and pores by using the ImageJ software. Firstly, the SEM image was converted into a binary image. Secondly, an appropriate threshold was set, and a variety of pore structure parameters (including total surface porosity) can be obtained. Moreover, organic surface porosity can be calculated within the zones of organic matter. The detailed analysis processes have been widely reported by previous authors [31,32]. The International Union of Pure and Applied Chemistry (IUPAC) classifies the pores of shale reservoirs as micropores (<2 nm), mesopores (2–50 nm), and macropores (>50 nm) [33] that were used for pore characterization in this study.

4. Results

The pores of the studied shale samples can be divided into three types: mineral matrix pores, organic pores, and micro-fractures, among which mineral matrix pores can be further subdivided into interparticle pores and intraparticle pores.

4.1. Mineral Matrix Pores

Mineral matrix pores were developed among mineral grains during deposition and diagenesis and can be divided into interparticle pores and intraparticle pores. Shale mineral grains generally include quartz, feldspar, calcite, pyrite, or their aggregates, and different types of pores may be formed among or within these different grains.

4.1.1. Interparticle Pores

Interparticle pores mainly refer to the unfilled pores that occurred at the contact point of inorganic mineral grains, commonly around rigid and brittle minerals, which are relatively developed in shallow shale reservoirs and have good pore connectivity, thus forming an effective pore network. In this study, interparticle pores are distributed in the shale mineral matrix, mostly on the edges of brittle mineral grains (e.g., quartz and feldspar). The edges and corners of detrital quartz grains are more distinct, and slit-shaped intergranular pores are formed along the edges of rigid grains, and pore size is generally in the range of 1.5–3.5 μm (Figure 2A,B). Biogenic quartz is usually presented as rounded micro-scaled quartz grains (so-called “microquartz”) (Figure 2C). Interparticle pores among these microquartz grains display triangular and angular shapes, which have wide variations in pore sizes, generally 0.1–3 μm . Overall, interparticle pores usually have the characteristics of good connectivity and wide variations in pore sizes, which are relatively developed.

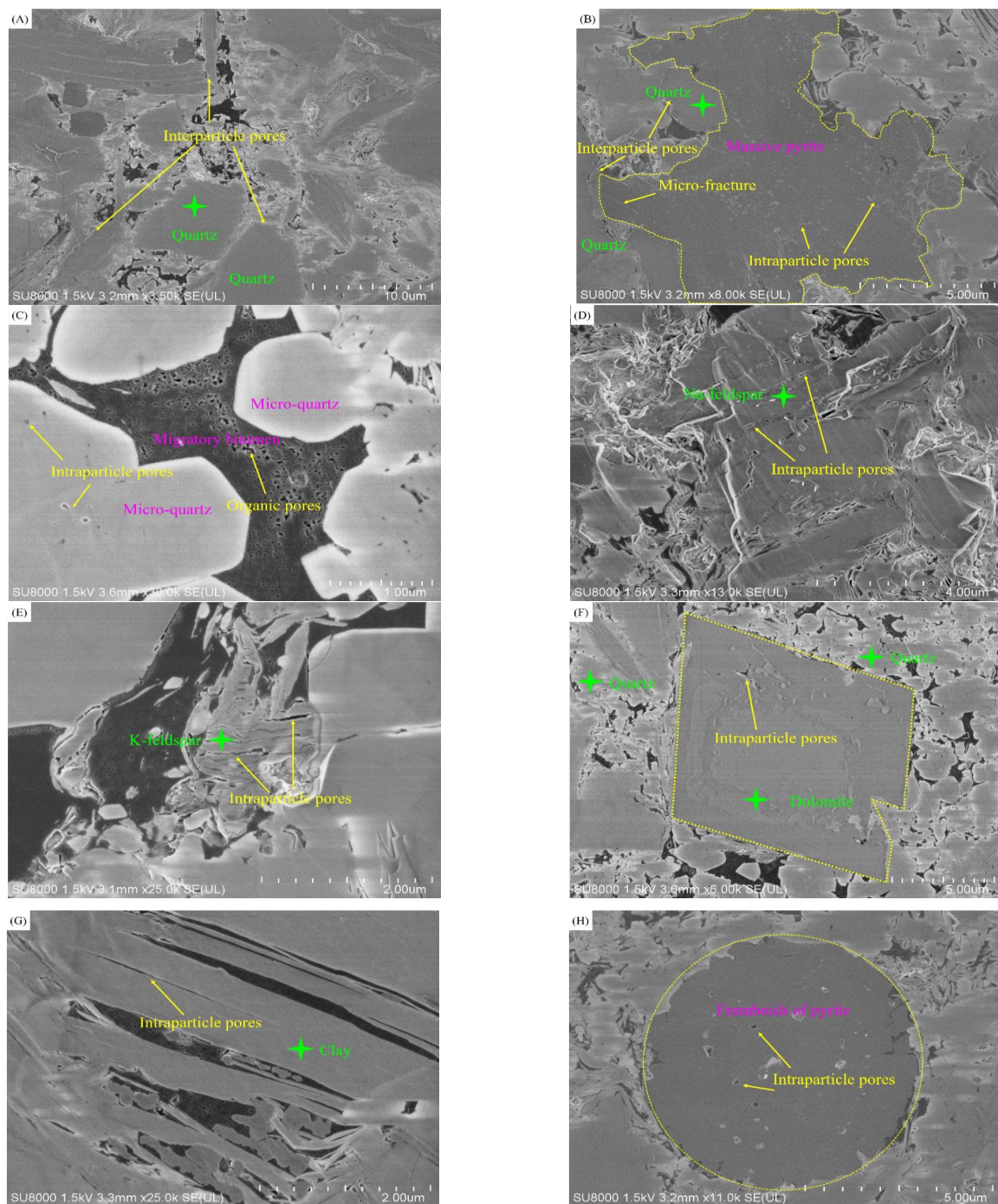


Figure 2. SEM photographs showing mineral-matrix pores of the studied WF-LMX shale samples. (A) slit-shaped interparticle pores were developed along the edges of brittle minerals; (B) interparticle pores were developed at the edges of quartz minerals, and intraparticle pores and micro-fractures can be observed within a massive pyrite grain; (C) isolated intraparticle pores can be observed within the interior of microquartz grains, and the pores between microquartz grains were filled with migrabitumen that hosted abundant nanopores; (D) intraparticle pores within an albite grain; (E) dissolution pores within the K-feldspar minerals; (F) irregular intraparticle pores within a dolomite grain; (G) the pores among clay platelets were filled by migrabitumen that hosted abundant nanopores; (H) some closed intraparticle pores within a framboidal pyrite grain. (Points delineated by green stars were analyzed by EDS).

4.1.2. Intraparticle Pores

Intraparticle pores can be observed within quartz, dolomite, feldspar, pyrite grains, and clay minerals in this study. Quartz is a stable mineral that is insoluble in acid solutions and slightly soluble in alkaline solutions. However, crystal lattice defects may be formed during the recrystallization of quartz, resulting in the formation of isolated globular and elliptical pores with poor connectivity and pore sizes generally ranging from 0.02 to 0.15 μm (Figure 2C). Feldspar is a brittle and unstable mineral that is prone to dissolution by organic acid fluids during hydrocarbon generation. Elliptical and short-column-shaped dissolution pores are often formed inside albite grains (Figure 2D). In K-feldspar grains, dissolution pores are also formed due to dissolution or lattice defects, which are mostly band-shaped (Figure 2E). At the diagenetic stage, another brittle mineral, dolomite, is easily dissolved by acidic fluids to form irregular dissolution holes. Some pore spaces can be filled by solid bitumen (Figure 2F). Clay minerals display banded or layered shapes, and the interlayer pores among clay minerals are prone to being elongated due to compaction and are sometimes filled with solid bitumen, with pore sizes ranging from 1.5 to 5.5 μm (Figure 2G). In the WF-LMX shale, a large number of framboidal or massive pyrite grains can be observed. Some single pyrite crystals are compact and irregularly overlapped, preventing the infilling of external solid bitumen and forming isolated intraparticle pores (Figure 2H). However, most intraparticle pores are still filled with solid bitumen, and a large number of organic pores are developed within solid bitumen, generally displaying square or oval shapes and pore sizes ranging from 0.045 to 0.35 μm (Figure 2H). In general, the intraparticle pores have the characteristics of small pore sizes and poor pore connectivity, so the contribution of intraparticle pores to the pore system of shale reservoirs is smaller than that of intergranular pores.

4.2. Organic Pores

Organic pores hosted in the OM grains are the most important pore type in the WF-LMX shale. A large number of organic zooclasts (such as graptolites and radiolarians) can be observed in the WF-LMX shale of the Sichuan Basin (Figure 3A,B). However, fewer pores were developed in the internal OM of graptolites and radiolarians, but more organic pores were developed in the solid bitumen generated around them (Figure 3A,B). Microorganisms, algae, and organic zooclasts generally generate oil and gas within shale reservoirs during thermal maturation. Liquid hydrocarbons can only migrate a very short distance in shale pore systems, and the migrated hydrocarbons can be retained in the mineral matrix pores (mainly interparticle pores). A large number of nanopores were developed in the retained solid bitumen. In particular, microquartz aggregates have a strong resistance to burial compaction, which can effectively resist the compaction during deep burials, thus providing a shield for the organic pores of the filling OM. The secondary organic pores mainly display bubble, honeycomb, and irregular shapes and a wide range of pore sizes, generally ranging from 0.02 to 0.65 μm , and abundant smaller pores can often be observed in the interior of large pores (Figure 3C). Such small-scaled pores form an effective channel with the surrounding large pores, enhancing the pore connectivity and increasing the specific surface area of organic pores, which are more conducive to the occurrence and accumulation of shale gas (Figure 3C). Due to the difference in kerogen types and different hydrocarbon generation potentials, strong heterogeneity of organic pores can be observed within the OM grains, including solid bitumen and graptolite (Figure 3D). The pores among clay platelets were generally filled with migrabitumen that hosted many nanopores. Influenced by the crystal morphology of clay minerals, the pores among clay platelets mostly display the narrow-long-shapes, and the long axis of the pores within the migrated solid bitumen is mostly parallel to the clay platelets (Figure 3E), while the short axis may indicate the direction of compaction or compression induced by tectonic activities. The intraparticle and interparticle pores between pyrite framboids were often filled by migrabitumen. Since pyrite is a rigid grain with strong resistance to burial compaction, a large number of pores are developed within the migrabitumen (Figure 3F).

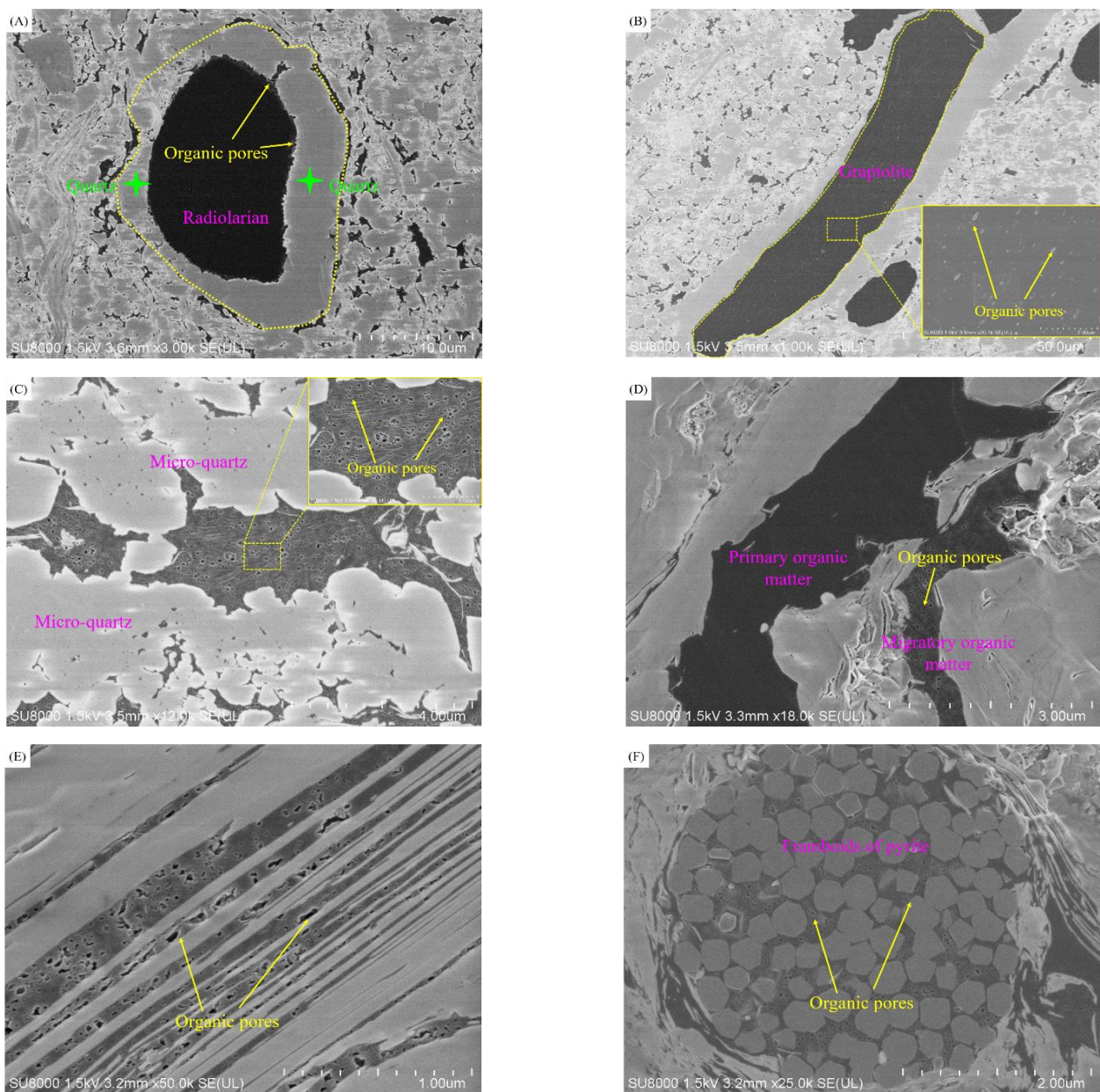


Figure 3. SEM photographs showing organic pores of the studied WF-LMX shale samples. (A) few pores were observed within the OM of a radiolarian, but numerous organic pores were visible at the edges of the OM; (B) few pores within the OM of a graptolite; (C) the interparticle pores of microquartz grains were filled with migrabitumen that hosted abundant nanopores; (D) the pores were less developed within the primary OM (probably kerogen), while the pores were well developed within the migrated OM (probably migrabitumen); (E) the pores among clay platelets were filled with migrabitumen that hosted abundant nanopores; (F) many organic pores developed within the migrabitumen occurred in the intraparticle pores of a framboidal pyrite grain. (Points delineated by green stars were analyzed by EDS).

Overall, organic pores were well developed and a most important pore type of the WF-LMX ultra-deep shale, which were of great significance to the accumulation, occurrence, and migration of shale gas.

4.3. Micro-Fractures

Micro-fractures are mainly developed at the contact edges between OM and mineral matrix and the interior of mineral grains in the WF-LMX ultra-deep shale. The micro-fractures at the contact edges between OM and detrital grains (quartz, feldspar, etc.) were formed due to the changes in the OM volume during hydrocarbon generation and the difference in stress intensity between OM and detrital grains during diagenesis (Figure 4A,B). With the increasing burial compaction, detrital grains are easily fractured to form micro-fractures. The micro-fractures within the interior of grains generally display flat and straight shapes, which are rarely filled by other minerals (Figure 4C). Feldspar grains are susceptible to dissolution, thus forming micro-fractures along the cleavage (Figure 4D). In general, micro-fractures can be connected with organic pores and interparticle pores to form a complex pore network, which can serve as both reservoir spaces and one of the major seepage channels for shale gas micro-migration.

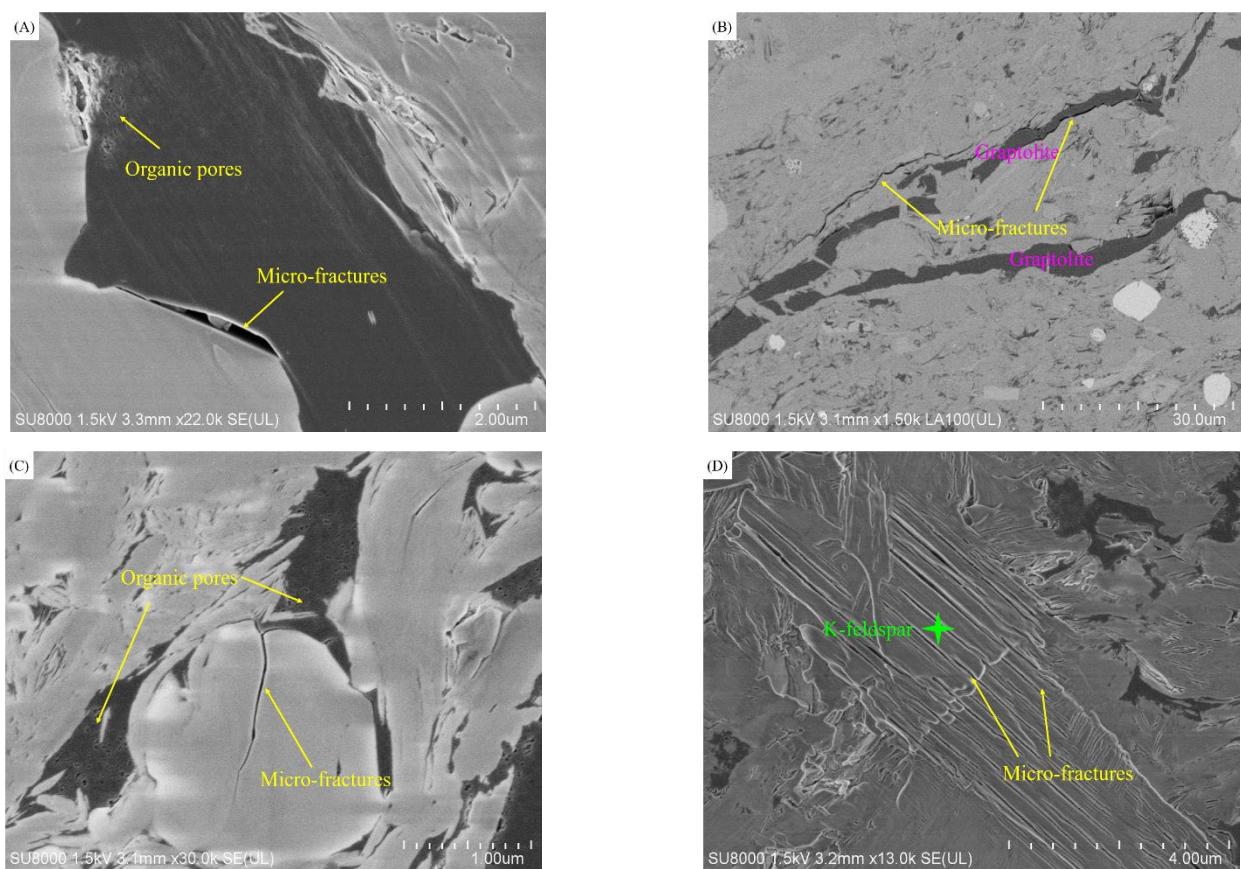


Figure 4. SEM photographs showing micro-fractures in the studied WF-LMX shale samples. (A) micro-fractures developed along the contact edges between OM and detrital grains; (B) micro-fractures developed along the contact edges between graptolite and surrounding minerals; (C) a relatively flat micro-fracture was developed within the interior of a microquartz grain; (D) a large number of micro-fractures were developed within the interior of a K-feldspar grain, which may be classified as cleavages. (Points delineated by green stars were analyzed by EDS).

4.4. Surface Porosity and Pore Structure

The total surface porosity of the studied WF-LMX shale samples was estimated to be in the range of 0.78–1.07%, with an average of 0.89%. Organic surface porosity was estimated to be in the range of 0.62–0.98%, with an average of 0.79%. The pore size distribution of organic pores ranges from 10 to 200 nm, which is mainly in the range of 5–45 nm, categorizing them as mesopores.

5. Discussions

5.1. Factors Controlling Pore Development and Preservation

Previous studies have shown that TOC contents and mineral compositions play important roles in the development and preservation of organic pores [34,35]. The increase in TOC content can promote the development of organic pores in shale reservoirs. Brittle minerals can provide a rigid framework for organic pore preservation, which can slow down the compaction process and promote organic pore preservation.

5.1.1. Total Organic Carbon Content

The effect of TOC content on pore structure parameters of shale reservoirs has been widely studied, and it is generally found that there is a good positive correlation between shale porosity (or pore volume) and TOC content. With increasing TOC content, the porosity and pore volume tend to increase, and the porosity is relatively developed within the OM grains [5,34,36].

In this study, total surface porosity and organic surface porosity of the WF-LMX ultra-deep shale samples show good positive correlations with TOC values (Figure 5), and no significant changes have occurred compared with mid-shallow shales, suggesting that TOC content is still the major factor controlling pore development of the WF-LMX ultra-deep shale. Organic pores are the major pore type in the studied WF-LMX shale reservoirs. During geological history, the shale OM was accumulated and buried to generate hydrocarbons. The higher the TOC content, the more micro- to nano-scaled organic pores were generated during hydrocarbon generation and expulsion processes, resulting in a more complex micro- to nano-scaled pore network of shale reservoirs. That is, the higher the TOC content, the more favorable the development of organic pores, and thus the greater the organic porosity. SEM observations have also shown that the pores of ultra-deep shale were mainly composed of organic pores (Figure 3), and the quantity of organic pores depended on the TOC contents. The surface porosity would be increased due to the increase in TOC contents, thus enhancing the adsorption and storage capacity of shale gas.

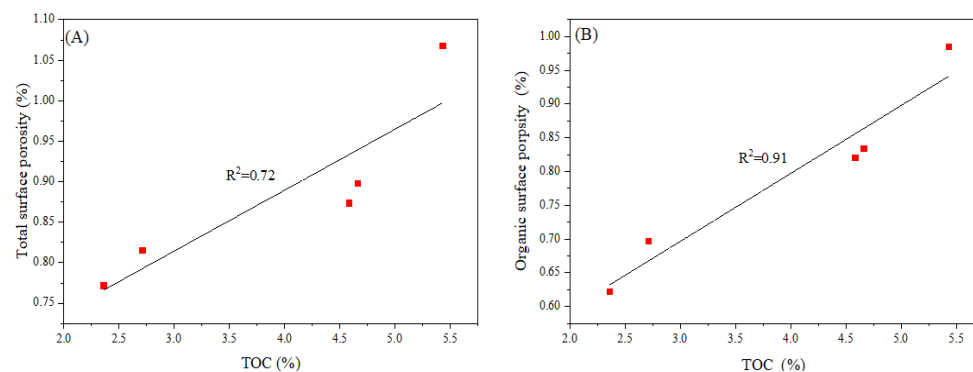


Figure 5. Cross-plots of TOC content versus (A) total surface porosity and (B) organic surface porosity of the WF-LMX ultra-deep shale samples from Well PS1.

5.1.2. Mineral Compositions

Mineral compositions also play a significant role in the pore development and preservation of shale reservoirs. Quartz and pyrite grains generally have strong compaction-resisting abilities, and interparticle pores among these rigid grains are easily preserved during burial, favoring shale gas storage [37]. Intraparticle pores are easily formed among the clay platelets, and these pores are well-connected and conducive to the storage and migration of shale gas. Thus, clay minerals are one of the major contributors to mineral matrix pores [38].

In this study, the total surface porosity of the WF-LMX ultra-deep shale samples showed a good positive correlation with quartz content (Figure 6A). Since the WF-LMX shale contains a large number of radiolarians, the interior OM of the radiolarians may have

a positive contribution to TOC content, thus leading to a good positive correlation between the quartz and TOC contents of the studied shale samples. The WF-LMX organic-rich siliceous shale generally contains a large number of microquartz grains, and the aggregates of microquartz grains can form a rigid framework to effectively resist burial compaction and avoid the collapse and compaction of organic pores (Figure 3C). At the same time, the interparticle pores among these microquartz grains can provide storage spaces for the migratbitumen during deep burials and strong compaction [27,36]. Thus, the organic pores of ultra-deep shale reservoirs can be largely preserved due to the widespread presence of authigenic quartz grains.

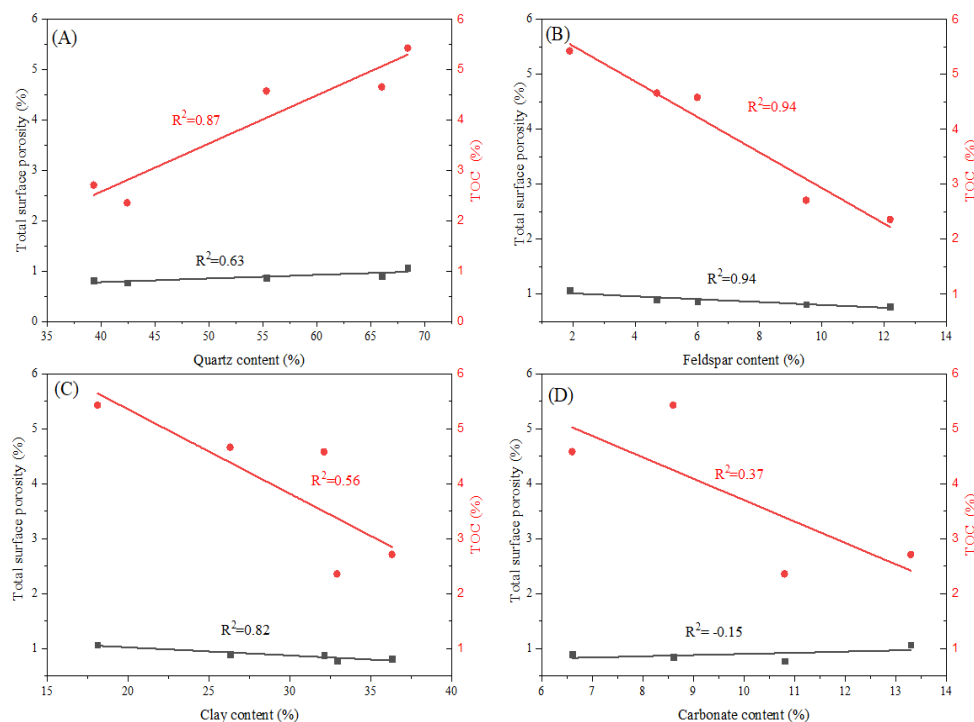


Figure 6. Cross-plots of total surface porosity and TOC content versus (A) quartz, (B) feldspar, (C) clay, and (D) carbonate contents of the WF-LMX ultra-deep shale samples from Well PS1.

The contents of feldspar minerals and clay minerals are roughly negatively correlated with the TOC contents of the studied shale samples, indicating that feldspar and clay minerals play a dilutive effect on TOC contents and thus are unfavorable for the development of nanopores. Thus, the total surface porosity of our studied shale samples is negatively correlated with the contents of feldspar and clay minerals (Figure 6B,C). The content of carbonate minerals in the WF-LMX shale samples is relatively low, and its influence on pore development is very limited, so no correlation between total surface porosity and carbonate content can be observed (Figure 6D).

5.2. Significance of Nanoscale Pores for Shale Gas Accumulation

In shale reservoirs, the intraparticle pores are usually scattered, and the pores are not connected, resulting in poor pore connectivity. The hydrocarbon fluids in the intraparticle pores, such as the intraparticle pores of quartz minerals and the dissolved pores of feldspar and carbonate grains, can enter the nanoscale channels through the matrix and then enter the larger micro-fractures, contributing to the permeability of shale reservoirs [39]. In the WF-LMX shale reservoirs, organic pores are the most important pore type, among which mesopores are the most abundant, and the adsorption capacity of shale gas is very strong. Organic nanopores become an important storage space for adsorbing natural gas. Abundant small-scale pores can often be observed inside some larger organic pores, which form an effective channel with the surrounding large pores and enhance the connectivity of

pore volume. At the same time, a complex pore network was formed in three-dimensional space, which controlled the occurrence and migration mechanism of shale gas [40,41]. In addition, micro-fractures are also the reservoir spaces of shale gas, which could serve as main channels of gas seepage. During the development of shale gas, micro-fractures can also promote shale gas production via artificial fracturing fractures.

5.3. Comparison with Mid-Shallow Shale Reservoirs

The pore structure characteristics of the WF-LMX mid-shallow shale reservoirs in Sichuan Basin and its neighboring areas have been extensively studied [42–44], and it has been found that the pore types of mid-shallow shale reservoirs include organic pores, interparticle pores, intraparticle pores, and micro-fractures. Among them, organic pores are the most important pore type, and they display bubble, ellipsoid, and slit shapes. The pore size distribution of organic pores mainly ranges from 10 to 100 nm, and organic pores with pore sizes larger than 100 nm are also developed. Since organic pores are the main reservoir spaces of shale gas reservoirs and have a great influence on the enrichment and production of shale gas [45,46], the comparison study of reservoir quality between ultra-deep shale and mid-shallow shale mainly focuses on the development of organic pores. The effect of burial compaction on organic pores in shale reservoirs is mainly reflected in the following two aspects: (1) pore morphology and (2) pore size distribution. Previous studies have shown that strong compaction can change the morphology of organic pores [47]. The morphology of organic pores in mid-shallow shale reservoirs includes mostly circular, elliptical, spongy, and irregular honeycomb shapes [48]. With the increasing burial depths, the circular pores gradually disappeared, and pore morphology gradually evolved into slit shapes (Figure 3E). Hu et al. [49] had reported that the diameter of organic pores in the WF-LMX mid-shallow shale samples from Well JY1 ranged from 5 to 1021 nm, with an average of 68 nm. Compared with well JY1, the organic pores of the studied WF-LMX shale samples from Well PS1 were still dominated by mesopores, but the pore size distribution tended to be relatively low, ranging from 5 to 40 nm. Moreover, organic pores larger than 100 nm in diameter were rarely developed in our studied ultra-deep shale samples (Figure 7). Therefore, organic pores would be gradually compacted with increasing burial depths, resulting in a reduction in pore size. The quantity of large organic pores in shale reservoirs from the shallow layer to the ultra-deep layer will gradually decrease. However, the WF-LMX shale reservoirs (especially siliceous shale) contain a large amount of authigenic microquartz grains, which can form a rigid framework to resist burial compaction, and organic pores hosted in solid bitumen could be preserved to some extent. Although the organic pores of ultra-deep shale reservoirs generally display relatively low sizes, they are still well developed, revealing significant potential for shale gas exploration.

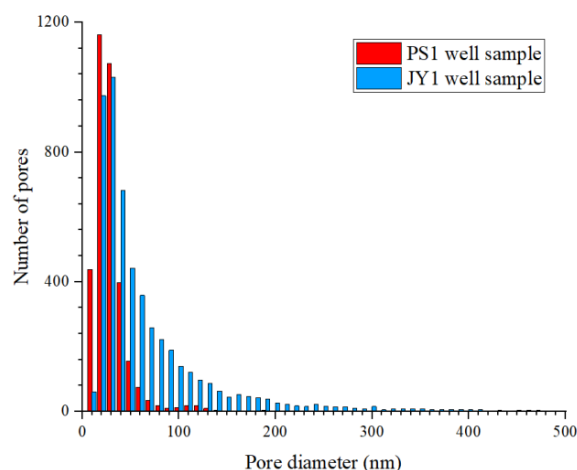


Figure 7. Comparison of organic pore size distribution between ultra-deep shale and mid-shallow shale of the WF-LMX in the Sichuan Basin (data for Well JY1 were from reference [49]).

6. Conclusions

- (1) The pore types of the WF-LMX ultra-deep shales in the Eastern Sichuan Basin include mineral matrix pores (interparticle pores and intraparticle pores), organic pores, and micro-fractures. Among them, organic pores are the most important pore type, and mesopores with pore sizes ranging from 5 to 45 nm are relatively developed. Mineral matrix pores are generally developed among the grains of quartz, pyrite aggregate and clay minerals, but they are generally filled by migrabitumen during hydrocarbon generation and expulsion, and a large number of organic pores are hosted in the retained solid bitumen. Organic pores can form a complex 3D pore network in shale reservoirs, which is conducive to the adsorption and storage of shale gas.
- (2) The development of pores in the WF-LMX ultra-deep shales is mainly controlled by TOC and quartz contents. A close association between abundant siliceous radiolarians and OM in the WF-LMX shale reservoirs implies that biogenic silica plays an important role in OM enrichments, thus favoring the development of organic pores. On the other hand, authigenic quartz belongs to a rigid mineral in shale reservoirs, which can avoid the collapse of organic pores to some extents due to burial compaction, and a large number of organic pores in ultra-deep shale can be preserved.
- (3) Organic pores are the main pore type in the WF-LMX ultra-deep shale reservoirs. Intergranular pores and microfractures can provide percolation channels and play an important role in hydrocarbon migration. Deep and ultra-deep shale has the characteristics of geological conditions of high temperature, high pressure, and high ground stress, as well as weak tectonic reconstructions. Natural fractures are less open, and the contribution of fractures to permeability is significantly reduced. Artificial improvement of the seepage capacity of deep shale reservoirs is very important to deep shale gas development. The shale intervals with high silica contents have strong anti-compaction abilities, which prevent organic pores from collapsing to a certain extent due to burial compaction and are conducive to the formation of effective reservoirs. Moreover, the brittle mineral quartz could also promote the formation of fractures induced by artificial fracturing. Therefore, the shale intervals with high contents of TOC and quartz are the “sweet-spots” of ultra-deep shale gas development.

Author Contributions: Conceptualization, R.C.; methodology, R.C.; software, J.D.; validation, Y.C.; resources, R.L.; writing—original draft preparation, R.C.; writing—review and editing, P.G.; supervision, P.G.; funding acquisition, P.G.; Conducting experiments, Q.Z. All authors have read and agreed to the published version of the manuscript.

Funding: This research was funded by the National Natural Science Foundation of China (grant numbers U19B6003-03-01 and 42272140) and the Innovation and Entrepreneurship Training Plan for College Students (grant number X202111415147).

Data Availability Statement: Not applicable.

Acknowledgments: All the editors and anonymous reviewers are gratefully acknowledged.

Conflicts of Interest: The authors declare no conflict of interest.

References

1. Jarvie, D.M.; Hill, R.J.; Ruble, T.E.; Pollastro, R.M. Unconventional shale-gas systems: The Mississippian Barnett Shale of northcentral Texas as one model for thermogenic shale-gas assessment. *AAPG Bull.* **2007**, *91*, 475–499. [[CrossRef](#)]
2. Nie, H.; Chen, Q.; Zhang, G.; Sun, C.; Wang, P.; Lu, Z. An overview of the characteristic of typical Wufeng–Longmaxi shale gas fields in the Sichuan Basin, China. *Nat. Gas Ind. B* **2021**, *8*, 217–230. [[CrossRef](#)]
3. Hao, F.; Zou, H.; Lu, Y. Mechanisms of shale gas storage: Implications for shale gas exploration in China. *AAPG Bull.* **2013**, *97*, 1325–1346. [[CrossRef](#)]
4. Qiu, Z.; Zou, C. Controlling factors on the formation and distribution of “sweet-spot areas” of marine gas shales in South China a preliminary discussion on unconventional petroleum sedimentology. *J. Asian Earth Sci.* **2020**, *194*, 103989. [[CrossRef](#)]

5. Xu, S.; Hao, F.; Shu, Z.; Zhang, A.; Yang, F. Pore structures of different types of shales and shale gas exploration of the Ordovician Wufeng and Silurian Longmaxi successions in the eastern Sichuan Basin, South China. *J. Asian Earth Sci.* **2020**, *193*, 104271. [[CrossRef](#)]
6. Curtis, M.E.; Cardott, B.J.; Sondergeld, C.H.; Rai, C.S. Development of organic porosity in the Woodford Shale with increasing thermal maturity. *Int. J. Coal Geol.* **2012**, *103*, 26–31. [[CrossRef](#)]
7. Curtis, J.B. Fractured shale-gas system. *AAPG Bull.* **2002**, *86*, 1921–1938.
8. Li, Z.; Lei, Z.; Shen, W.; Martyushev, D.A.; Hu, X. A Comprehensive Review of the Oil Flow Mechanism and Numerical Simulations in Shale Oil Reservoirs. *Energies* **2023**, *16*, 3516. [[CrossRef](#)]
9. Chalmers, G.R.; Bustin, R.M.; Power, I.M. Characterization of gas shale pore systems by porosimetry, pycnometry, surface area, and field emission scanning electron microscopy/transmission electron microscopy image analyses: Examples from the Barnett, Woodford, Haynesville, Marcellus, and Doig units. *AAPG Bull.* **2012**, *96*, 1099–1119.
10. Katz, B.J.; Arango, I. Organic porosity: A geochemist's view of the current state of understanding. *Org. Geochem.* **2018**, *123*, 1–16. [[CrossRef](#)]
11. Mastalerz, M.; Schimmelmann, A.; Drobniak, A.; Chen, Y. Porosity of Devonian and Mississippian New Albany Shale across a maturation gradient: Insights from organic petrology, gas adsorption, and mercury intrusion. *AAPG Bull.* **2013**, *97*, 1621–1643. [[CrossRef](#)]
12. Slatt, R.M.; O'Brien, N.R. Pore types in the Barnett and Woodford gas shales: Contribution to understanding gas storage and migration pathways in fine-grained rocks. *AAPG Bull.* **2011**, *95*, 2017–2030. [[CrossRef](#)]
13. Loucks, R.G.; Reed, R.M.; Ruppel, S.C.; Hammes, U. Spectrum of pore types and networks in mudrocks and a descriptive classification for matrix-related mudrock pores. *AAPG Bull.* **2012**, *96*, 1071–1098. [[CrossRef](#)]
14. Milliken, K.L.; Rudnicki, M.; Awwiller, D.N.; Zhang, T. Organic matter-hosted pore system, Marcellus Formation (Devonian), Pennsylvania. *AAPG Bull.* **2013**, *97*, 177–200. [[CrossRef](#)]
15. Loucks, R.G.; Reed, R.M.; Ruppel, S.C.; Jarvie, D.M. Morphology, genesis and distribution of nanometer-scale pores in siliceous mudstones of the Mississippian Barnett Shale. *J. Sed. Res.* **2009**, *79*, 848–861. [[CrossRef](#)]
16. Nie, H.; Zhang, J.; Jiang, S. Types and characteristics of the lower Silurian shale gas reservoirs in and around the Sichuan Basin. *Acta Geol. Sin.* **2015**, *89*, 1973–1985.
17. Ma, X.; Xie, J.; Yong, R.; Zhu, Y. Geological characteristics and high production control factors of shale gas reservoirs in Silurian Longmaxi Formation, southern Sichuan Basin, SW China. *Pet. Explor. Dev.* **2020**, *47*, 901–915. [[CrossRef](#)]
18. Dai, J.; Ni, Y.; Qin, S.; Huang, S.; Peng, W. Geochemical characteristics of ultra-deep natural gas in the Sichuan Basin, SW China. *Pet. Explor. Dev.* **2018**, *45*, 619–628. [[CrossRef](#)]
19. Guo, T.; Zhang, H. Formation and enrichment mode of Jiaoshiba shale gas field, Sichuan Basin. *Pet. Explor. Dev.* **2014**, *41*, 31–40. [[CrossRef](#)]
20. Nie, H.; Jin, Z.; Li, P.; Jay Katz, B.; Dang, W.; Liu, Q. Deep shale gas in the Ordovician-Silurian Wufeng-Longmaxi formations of the Sichuan Basin, SW China: Insights from reservoir characteristics, preservation conditions and development strategies. *J. Asian Earth Sci.* **2023**, *244*, 105521. [[CrossRef](#)]
21. Jin, Z.; Nie, H.; Liu, Q.; Zhao, J. Source and seal coupling mechanism for shale gas enrichment in upper Ordovician Wufeng Formation-Lower Silurian Longmaxi Formation in Sichuan Basin and its periphery. *Mar. Petrol. Geol.* **2018**, *97*, 78–93. [[CrossRef](#)]
22. Long, S.; Feng, D.; Li, F.; Du, W. Prospect analysis of the deep marine shale gas exploration and development in the Sichuan Basin, China. *J. Nat. Gas Geosci.* **2018**, *3*, 181–189. [[CrossRef](#)]
23. He, Z.; Nie, H.; Hu, D.; Jiang, T.; Wang, R.; Zhang, Y.; Zhang, G. Geological problems in the effective development of deep shales gas: A case study of Upper Ordovician Wufeng-Lower Silurian Longmaxi Formation in Sichuan Basin and its periphery. *Acta Petrol. Sin.* **2020**, *41*, 379–391, (In Chinese with English Abstract)
24. Gao, P.; Xiao, X.; Hu, D.; Liu, R.; Li, F. Gas in place and its controlling factors of deep shale of the Wufeng-Longmaxi formations in the Dingshan area, Sichuan Basin. *Front. Earth Sci.* **2023**, *17*, 322–336. [[CrossRef](#)]
25. Gao, P.; Xiao, X.; Hu, D.; Liu, R.; Cai, Y.; Yuan, T. Water distribution in the ultra-deep shale of the Wufeng-Longmaxi Formations from the Sichuan Basin. *Energies* **2022**, *15*, 2215. [[CrossRef](#)]
26. Guo, X.; Hu, D.; Huang, R.; Wei, Z.; Duan, J. Deep and ultra-deep natural gas exploration in the Sichuan Basin: Progress and prospect. *Nat. Gas Ind. B.* **2020**, *7*, 419–432. [[CrossRef](#)]
27. Gao, P.; Xiao, X.; Hu, D. Effect of silica diagenesis on porosity evolution of deep gas shale reservoir of the Lower Paleozoic Wufeng-Longmaxi formations, Sichuan Basin. *Mar. Pet. Geol.* **2022**, *145*, 105873. [[CrossRef](#)]
28. Wang, Y.; Liu, L.; Zheng, S.; Luo, Z.; Sheng, Y.; Wang, X. Full-scale pore structure and its controlling factors of the Wufeng-Longmaxi shale, southern Sichuan Basin, China: Implications for pore evolution of highly overmature marine shale. *J. Nat. Gas Sci. Eng.* **2019**, *67*, 134–146. [[CrossRef](#)]
29. He, X.; Chen, G.; Wu, S.; Zhang, J.; Zhang, X. Deep shale gas exploration and development in the southern Sichuan Basin: New progress and challenges. *Nat. Gas Ind. B.* **2023**, *10*, 32–43. [[CrossRef](#)]
30. Ma, X.; Wang, H.; Zhou, S.; Shi, Z. Deep shale gas in China: Geological characteristics and development strategies. *Energy Rep.* **2021**, *7*, 1903–1914. [[CrossRef](#)]
31. Rine, J.M.; Smart, E.; Dorsey, W. Comparison of porosity distribution within selected north American shale units by SEM examination of argon-ion-milled samples. *Electron Microsc. Shale Hydrocarb. Reserv. AAPG Mem.* **2013**, *102*, 137–152.

32. Pszonka, J.; Götze, J. Quantitative estimate of interstitial clays in sandstones using Nomarski differential interference contrast (DIC) microscopy and image analysis. *J. Pet. Sci. Eng.* **2018**, *161*, 582–589. [[CrossRef](#)]
33. Thommes, M.; Kaneko, K.; Neimark, A.V.; James, P.O.; Francisco, R.-R. Physisorption of gases, with special reference to the evaluation of surface area and pore size distribution (IUPAC Technical Report). *Pure Appl. Chem.* **2015**, *87*, 1051–1069. [[CrossRef](#)]
34. Guo, T.; Meng, X.; Lei, W.; Liu, M.; Huang, L. Characteristics and Governing Factors of Pore Structure and Methane Sorption in Deep-Marine Shales: A Case Study of the Wufeng–Longmaxi Formations, Weirong Shale Gas Field, Sichuan Basin. *Nat. Resour. Res.* **2023**, *32*, 1733–1759. [[CrossRef](#)]
35. Lu, H.; Zhao, A.; Lu, L.; Jiang, L. Pore Characterization and Its Controlling Factors in the Wufeng-Longmaxi Shale of North Guizhou, Southwest China. *Energy Fuels* **2020**, *34*, 15763–175722. [[CrossRef](#)]
36. Chen, L.; Jiang, Z.; Liu, Q.; Jiang, S.; Liu, K.; Tan, J. Mechanism of shale gas occurrence: Insights from comparative study on pore structures of marine and lacustrine shales. *Mar. Pet. Geol.* **2019**, *104*, 200–216. [[CrossRef](#)]
37. Zheng, X.; Zhang, B.; Sanei, H.; Bao, H.; Meng, Z.; Wang, Z. Pore structure characteristics and its effect on shale gas adsorption and desorption behavior. *Mar. Pet. Geol.* **2019**, *100*, 165–178. [[CrossRef](#)]
38. Wang, Q.; Lu, H.; Wang, T.; Liu, D.; Peng, P.; Zhan, X. Pore characterization of Lower Silurian shale gas reservoirs in the Middle Yangtze region, central China. *Mar. Pet. Geol.* **2018**, *89*, 14–26. [[CrossRef](#)]
39. O'Brien, N.R.; Thyne, G.; Slatt, R.M. Morphology of hydrocarbon droplets during migration: Visual example from the Monterey Formation (Miocene), California. *AAPG Bull.* **1996**, *80*, 1710–1718.
40. Chen, S.; Zhu, Y.; Wang, H.; Liu, H.; Wei, W. Structure characteristics and accumulation significance of nanopores in Longmaxi shale gas reservoir in the southern Sichuan Basin. *J. China Coal Soc.* **2012**, *37*, 438–444, (In Chinese with English Abstract).
41. Yang, F.; Ning, Z.; Hu, C.; Wang, B.; Peng, K. Characterization of microscopic pore structures in shale reservoirs. *Acta Pet. Sinica.* **2013**, *34*, 301–311, (In Chinese with English Abstract)
42. Shao, X.; Pang, X.; Li, Q.; Wang, P.; Chen, D.; Shen, W.; Zhao, Z. Pore structure and fractal characteristics of organic-rich shales: A case study of the lower Silurian Longmaxi shales in the Sichuan Basin, SW China. *Mar. Pet. Geol.* **2017**, *80*, 192–202. [[CrossRef](#)]
43. Xiong, J.; Li, Y.; Zhou, S.; Liu, X.; Han, H.; Liang, L. Insights into the pore structure characteristics of the Lower Silurian Longmaxi Formation shale in the Jiaoshiba area, Southern Sichuan Basin, China. *J. Pet. Explor. Prod. Technol.* **2022**, *12*, 2857–2868. [[CrossRef](#)]
44. Chen, Z.; Song, Y.; Jiang, Z.; Liu, S.; Li, Z. Identification of organic matter components and organic pore characteristics of marine shale: A case study of Wufeng-Longmaxi shale in southern Sichuan Basin, China. *Mar. Pet. Geol.* **2019**, *109*, 56–69. [[CrossRef](#)]
45. Zhao, Y.; Gao, P.; Zhou, Q.; Xiao, X. A review of the heterogeneity of organic-matter-hosted pores in shale reservoirs. *Energies* **2022**, *15*, 8805. [[CrossRef](#)]
46. Nie, H.; Zhang, G.; Li, P.; Ding, J.; Dang, W. Research status and prospect on organic matter pores in shale. *Acta Pet. Sinica.* **2022**, *43*, 1770–1787, (In Chinese with English Abstract)
47. Jiao, K.; Ye, Y.; Liu, S.; Ran, B.; Deng, B.; Li, Z. Characterization and Evolution of Nanoporosity in Superdeeply Buried Shales: A Case Study of the Longmaxi and Qiongzhusi Shales from MS Well #1, North Sichuan Basin, China. *Energy Fuels* **2018**, *32*, 191–203.
48. Yang, R.; He, S.; Hu, D.; Zhang, H.; Zhang, J. Characteristics and the main controlling factors of micro-pore structure of the shale in Wufeng Formation-Longmaxi Formation in Jiaoshiba area. *Geol. Sci. Technol. Inf.* **2015**, *34*, 105–113, (In Chinese with English Abstract)
49. Hu, H.; Hao, F.; Lin, J.; Lu, Y.; Ma, Y.; Li, Q. Organic matter-hosted pore system in the Wufeng-Longmaxi (O3w-S11) shale, Jiaoshiba area, Eastern Sichuan Basin, China. *Int. J. Coal Geol.* **2017**, *173*, 40–50. [[CrossRef](#)]

Disclaimer/Publisher’s Note: The statements, opinions and data contained in all publications are solely those of the individual author(s) and contributor(s) and not of MDPI and/or the editor(s). MDPI and/or the editor(s) disclaim responsibility for any injury to people or property resulting from any ideas, methods, instructions or products referred to in the content.